sustainability

MDPI

Article

Improving Spatial Soil Moisture Representation through the Integration of SMAP and *PROBA-V* Products

Shu-Di Fan [1,2,3,4], Yue-Ming Hu [1,2,3,4,5,*], Lu Wang [1,*], Zhen-Hua Liu [1,2,3,4], Zhou Shi [9], Wen-Bin Wu [10], Yu-Chun Pan [11], Guang-Xing Wang [2,3,4,6], A-Xing Zhu [2,3,4,8] and Bo Li [1,7]

1 College of Natural Resources and Environment, South China Agricultural University, Guangzhou 510642, China; fsd_1990@126.com (S.-D.F.); grassmoutain@163.com (Z.-H.L.); bli@cse.ust.hk (B.L.)
2 Key Laboratory of Construction Land Transformation, Ministry of Land and Resources, South China Agricultural University, Guangzhou 510642, China; gxwang@siu.edu (G.-X.W.); azhu@wisc.edu (A.-X.Z.)
3 Guangdong Provincial Key Laboratory of Land Use and Consolidation, South China Agricultural University, Guangzhou 10642, China
4 Guangdong Province Engineering Research Center for Land Information Technology, South China Agricultural University, Guangzhou 510642, China
5 School of Resources and Environment, University of Electronic Science of China, Chengdu 610054, China
6 Department of Geography and Environmental Resources, College of Liberal Arts, Southern Illinois University Carbondale (SIUC), Carbondale, IL 62901, USA
7 Department of Computer Science and Engineering, Hong Kong University of Science and Technology, Hong Kong 999077, China
8 Department of Geography, University of Wisconsin, Madison, WI 53706, USA
9 Institute of Agricultural Remote Sensing & Information System, Zhejiang University, Hangzhou 310029, China; shizhou@zju.edu.cn
10 Institute of Agricultural Resources and Regional Planning, Chinese Academy of Agricultural Sciences, Beijing 100081, China; wwbyn@yahoo.com
11 Beijing Research Center for Information Technology in Agriculture, Beijing 100097, China; panyc@nercita.org.cn
* Correspondence: ymhu163@163.com (Y.-M.H.); selinapple@163.com (L.W.)

Received: 28 June 2018; Accepted: 23 September 2018; Published: 28 September 2018

Abstract: To increase the spatial resolution of Soil Moisture Active Passive (SMAP), this study modifies the downscaling factor model based on the Temperature Vegetation Drought Index (*TVDI*) using data from the Project for On-Board Autonomy (*PROBA-V*). In the modified model, *TVDI* parameters were derived from the temperature-vegetation space and the Enhanced Vegetation Index (EVI). This study was conducted in the north China region using SMAP, *PROBA-V*, and Moderate Resolution Imaging Spectroradiometer satellite images. The 9-km spatial resolution SMAP data was downscaled to 0.3-km spatial resolution soil moisture using a modified downscaling method. Downscaling accuracies from the original and modified downscaling factor models were compared based on field observations. The results show that both methods generated similar spatial distributions in which soil moisture estimates increased as vegetation coverage increased from built-up areas to forest. However, based on the root mean square error between observations and estimations, the modified model demonstrated an increased estimation accuracy of 4.2% for soil moisture compared to the original method. This study also implies that downscaled soil moisture shows promise as a data source for subsequent watershed scale studies.

Keywords: soil moisture; temperature vegetation drought index; downscaling; SMAP; *PROBA-V*

1. Introduction

Soil moisture is a key variable in hydrogeological monitoring; it can reflect infiltration and runoff, thus indicating precipitation distribution in the region [1,2]. Soil moisture controls the balance of surface energy and influences atmosphere formation through latent heat flux and sensible heat flux. In agricultural management, soil moisture content is an important measure of rational water resource utilization. In hydrological models, climate models, and agricultural management, soil moisture is entered the model as a parameter.

Soil moisture parameter acquisition mainly involves remote sensing optical data (e.g., Aqua satellite) and microwave remote sensing data (e.g., Soil Moisture and Ocean Salinity satellite). The inversion data is the surface parameters obtained by the algorithm through the band information of the image. Optical data have high spatial resolution, which can meet the spatial resolution requirements of research, but inversion accuracy is not high due to the influence of weather factors and the vegetation canopy [3–5]. In passive microwave remote sensing, Soil Moisture Active Passive (SMAP) at the L-band can penetrate the soil surface and obtain high-precision data products [6,7]. However, these data demonstrate low spatial resolution, which can be improved via a downscaling process.

The spatial resolution of soil moisture data based on the L-band (i.e., passive microwave) cannot satisfy watershed scale studies. Therefore, it is essential to identify a simple and feasible downscaling approach for this problem. Several downscaling methods have been developed throughout the past decade, which can be classified into three categories: (i) regression methods based on the use of topography and soil depth information [8,9]; (ii) methods based on the combination of coarse resolution passive microwave data with fine-scale optical data and a surface process model [10]; and (iii) methods based on the combination of passive microwave data with a downscaling factor, such as the Surface Temperature and Vegetation Index [11].

The regression method involves scale conversion by establishing the functional relation of the characteristic quantities (e.g., vegetation index, land surface area, and surface temperature) of different images [12,13]. This method retains the integrity of image radiation information while reducing scale, which benefits the application of results in other models [14]. However, this class of methods must follow the premise that the functional relation is essentially identical on all scales [15]; in addition, functional relationships must be determined through a single land-cover type.

Methods based on fine-scale optical data and a surface process model must obtain the evaporative fraction (EF) and actual evaporative fraction (AEF), which are used in the energy balance model. Then, the method is implemented using a surface energy balance model to decouple the effects of external factors (i.e., land use, soil depth, and meteorological forcing) on the relationships between the parameters of the energy balance model and surface soil moisture. These methods comprehensively consider land-cover type, soil evaporation efficiency, and non-linear relationships, rendering the results of pixel decomposition more similar to the actual value with an error of 0.012 m^3/m^3. However, these methods must obtain additional parameters to support accurate scaling results, and complex calculations are required. In practical applications, these methods are highly accurate, but do not meet hydrogeological monitoring requirements due to the operational complexity [16–18].

Methods based on a combination of passive microwave data and downscaling factors consider the surface temperature and vegetation coverage index and establish the relative soil moisture index, but have two fundamental differences [19]: (i) it is unnecessary to have an EF and AEF; and (ii) a simple energy balance model can be used in place of a complex surface process model. Given the assumption that the soil moisture and humidity index functions are identical under different conditions (i.e., spatial resolution), then the spatial resolution of soil moisture can be improved through scaling factor calculations. The parameters in downscaling factor methods are independent of ground data, and are characterized by simple operation and high efficiency [20]. This method has been shown to be applicable to semi-arid regions [11], and does not need to consider the effect of land-cover type on interpolation results.

Given these approaches, the problem to be solved involves the application of an appropriate downscaling method to SMAP data to satisfy downscaling data in watershed scale research. The research in this aspect has certain research foundations, but there are some imperfections that need further study. The objectives of this study are hence to (1) establish the Temperature Vegetation Drought Index (*TVDI*) based on the downscaling factor method to improve the spatial resolution of SMAP soil moisture products in the study area; and (2) assess the accuracy of downscaling associated with various land uses.

2. Material and Method

2.1. Study Site and Data

The north China region belongs to a natural geographic region, referring to the northern part of the Qinling Mountains-Huaihe River Line and the southern part of the Great Wall. The study area was in north China between 109°39′03″–120°54′40″ E and 34°20′17″–46°40′48″ N. The study area includes five provinces (Beijing, Tianjin, Hebei, Shanxi, and Central Inner Mongolia) and covers a total area of 386,401.77 km^2 (Figure 1). With a semi-humid climate, light conditions in north China are abundant; the winter is cold, dry, and long; the surface temperature in summer is high; and precipitation is relatively heavy [21]. The soil type in this area is brown soil, which mainly produces wheat. The land-use type in the research area is mostly grassland and cropland, accounting for more than 70% of the total area. Cropland is distributed in the North China Plain, whereas grassland is mainly distributed on the Loess Plateau. Woodland appears in the central part of Hebei province and southern part of Shanxi Province. Construction land is mainly distributed around the capital cities of Beijing and Tianjin (Table 1). The image layer was set to the Universal Transverse Mercator (UTM) coordinate system, which is the coordinate system for all of the data that is used in this study. The land-use image was divided into 500 × 500 m grids, which were used to analyze the spatial distribution characteristics of temperature and vegetation cover. The land use in each grid was determined by the dominant land-use type, because the type of land in a grid may contain multiple land uses.

In this study, SMAP Level-3 (L3) soil moisture product from May 2016 to May 2017 were obtained as a baseline for data downscaling, which provided a composite of daily estimates of global land surface conditions retrieved by the Soil Moisture Active Passive (SMAP) radiometer. In order to cover the study area, three days of synthetic images were used as the basic data [22]. SMAP observations further improved soil moisture assimilation estimates, because SMAP operates at the L-band, whereas Advanced Microwave Scanning Radiometer (AMSRE) and Advanced Scattermeter (ASCAT) retrievals are based on the X-band (10.7 GHz) and C-band (5.3 GHz), respectively. SMAP offers observations at higher resolutions that are less affected by radiofrequency interference than those from soil moisture and ocean salinity (SMOS) [23]. Project for On-Board Autonomy (*PROBA-V*) data and Moderate Resolution Imaging Spectroradiometer (*MODIS*) data were used to calculate the downscaling factor in the downscaling process. This study used annual average of Daily composite (S1) Top of Canopy *PROBA-V* (TOC) data on between 1–3 May in 2016 and 2017 in the soil moisture downscaling process, which registered in four spectral bands: blue (centered at 0.463 μm), red (0.655 μm), near-infrared spectrum (NIR; 0.837 μm), and shortwave (length) infrared spectral bands (SWIR; 1.603 μm). Observations were taken at resolutions between 100–180 m at nadir up to 350 m and 660 m at the swath extremes for the VNIR (visible and near-infrared) and SWIR channels, respectively [24]. Table 2 lists the radiometric characteristics of the *PROBA-V* spectral bands. Intersensor differences in the individual band reflectance and the Normalized Difference Vegetation Index (*NDVI*) are summarized in Table 3.

Differences were identified between the individual spectra, which were largest for the SWIR band. For the NIR and red bands, differences between *PROBA-V* and VGT-1 were of the same order of magnitude as those of VGT2-VGT1, leading to similar *NDVI* differences. By contrast, the SWIR channel differences compared to VGT2-VGT1 were three times larger.

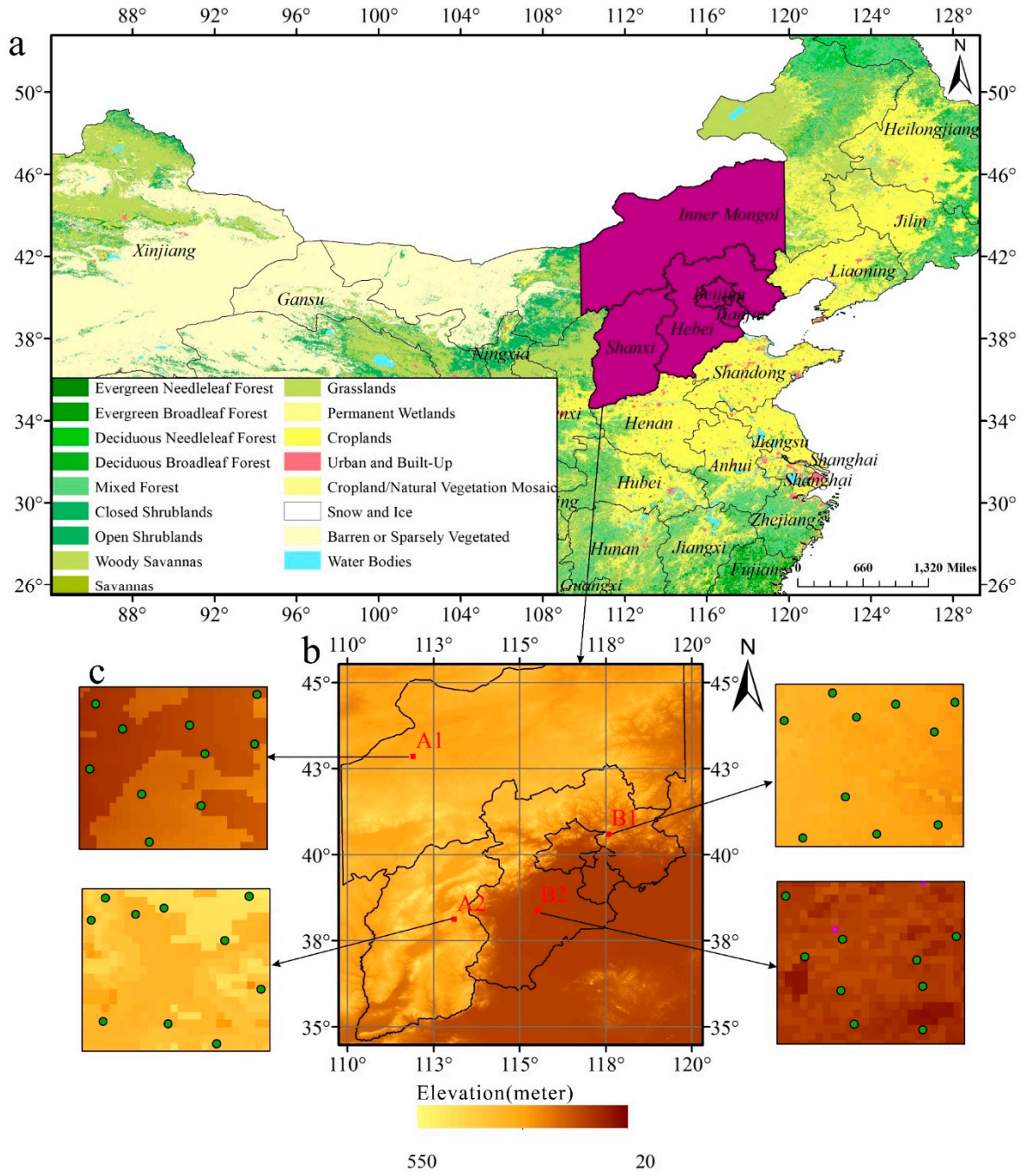

Figure 1. (**a**) Location of (**b**) the study site shown in grayscale from Soil Moisture Active Passive (SMAP) data, and (**c**) spatial distribution of sample plot (sample for validating estimated soil moisture). Data source: Western China Environmental and Ecological Science Data Center.

For *MODIS*, the annual average data of MOD11A1 and MOD13Q1 from May 2016 to May 2017 were obtained from the National Snow and Ice Data Center (NSIDC) Distributed Data Archive [25] and used as the basic data product to build downscaling factors. The *MODIS* were based on Terra and Aqua and contained 36 spectral bands, including visible and infrared wavelengths. MOD11A1 denoted the surface temperature product of the *MODIS* Terra satellite, namely grid data organized by tiles. The projection was sinusoidal, with daily time resolution and a spatial resolution of 0.93 km. MYD13Q1 data consisted of a 250-m L3 data products with a sinusoidal projection containing the Enhanced Vegetation Index (EVI); the effects of aerosols were corrected through the blue band.

Table 1. Land cover situation in study area.

Value	Land Use	Count	Area (km·km)	Percent (%)
1	Evergreen Needle Leaf Forest	1934	1133.07	0.29%
2	Evergreen Broadleaf Forest	2168	1270.17	0.33%
3	Deciduous Needle Leaf Forest	5223	3060.00	0.79%
4	Deciduous Broadleaf Forest	18,874	11,057.71	2.86%
5	Mixed Forest	51,534	30,192.22	7.81%
6	Closed Shrublands	7328	4293.26	1.11%
7	Open Shrublands	15,959	9349.90	2.42%
8	Woody Savannas	3822	2239.20	0.58%
9	Savannas	14,820	8682.59	2.25%
10	Grasslands	249,424	146,130.04	37.82%
11	Permanent Wetlands	284	166.39	0.04%
12	Croplands	239,739	140,455.89	36.35%
13	Urban and Built-Up	20,759	12,162.08	3.15%
14	Cropland/Natural Vegetation Mosaic	5192	3041.84	0.79%
15	Snow and Ice	330	193.34	0.05%
16	Barren or Sparsely Vegetated	17,761	10,405.64	2.69%
17	Water Bodies	4384	2568.45	0.66%
Total		659,535	386,401.77	100.00%

Table 2. Project for On-Board Autonomy (*PROBA-V*) spectral and radiometric characteristics.

Band Name	Centre Wavelength (μm)	Spectral Range (μm)	Signal Noise Ratio and Irradiance
BLUE	0.464	0.440–0.487	177,111
RED	0.655	0.614–0.696	598,110
NIR	0.837	0.772–0.902	574,106
SWIR	1.603	1.570–1.635	72,020
Radiometric performance			
Absolute accuracy (%)		<5	
Inter-channel accuracy (%)		<3	
Stability (%)		<3	
Geometric performance			
Geolocation mean accuracy (standard deviation) (m)		BLUE:69.69 (49.94) RED:60.46 (50.78) NIR:61.30 (50.52) SWIR:61.86 (50.03)	

Data source: http://www.vito-eodata.be/.

Table 3. Average relative difference (%) in band reflectance and Normalized Difference Vegetation Index (*NDVI*) between VGT2 (Vegetation sensor 2) and VGT1 (Vegetation sensor 1), *PROBA-V* and VGT1, and *PROBA-V* and VGT2.

Relative Difference	VGT2-VGT1	*PROBA-V*-VGT1	*PROBA-V*-VGT2
BLUE	−0.13	1.98	2.11
RED	−3.20	−3.91	−0.74
NIR	0.29	−0.47	−0.76
SWIR	−1.37	−4.65	−3.37
NDVI	3.68	3.34	−0.33

2.2. Data Preprocessing

Land use in the study area was classified using remote sensing image classification in the study area. *MODIS* images acquired in May 2017 as a spatial resolution of 0.5 km were sourced for image classification. The classification system developed by the International Geosphere-Biosphere Programme (IGBP) was adopted to classify the research into 17 categories [26,27]. Land-use

extraction was achieved through the object-oriented classification [28–30] module in ENVI5.3 software (Exelis Visual Information Solutions, Inc., Broomfield, CO, USA).

The geographic coordinates of the three data sources were inconsistent; the *MODIS* and *PROBA-V* coordinate system used the World Geodetic System 1984 (WGS84), while the SMAP product was the Cylindrical Equal-area coordinate system. The first step was to re-project the SMAP product from Cylindrical Equal-area to WGS84, and modify the output GeoTIFF file to be ingestible into commonly used GIS applications. After completing the coordinate transformation, the next step is to resample the data so that the three types of data (*MODIS*, *PROBA-V*, and SMAP) are the same pixel size for the model. Since the map of *PROBA-V* data is small, the adjacent four images need to be spliced by seamless mosaic algorithm before resampling. After resampling, the spatial resolution of all three data is 297.661 m (≈0.3 km). To eliminate the abnormal values of the data in the study area, it is necessary to specify a (2, n) array of one or more data ranges for inputting mask data values, where n is the number of data ranges. Each pixel within the data range will not be masked. Then, a unique data value for pixels needs to be specified in the output raster that have a non-zero pixel state value.

The next steps involve geometric correction; using the Image Registration workflow geometrically aligns images with different viewing geometry and/or different terrain distortions into the same coordinate system so that corresponding pixels represent the same objects. In order to eliminate the influence of atmosphere on image data, FLAASH (Fast Line-of-sight Atmospheric Analysis of Spectral Hypercubes) atmospheric correction based on the MODTRAN5 radiation transport (RT) model was used in this study. According to the latitude and terrain of the study area, atmospheric model and aerosol model were Sub-Arctic Summer (SAS) and Urban, respectively, and the aerosol retrieval method was 2-band (Kauth-Thomas Transformation).

The last step of preprocessing is to mask the raster of SMAP, *PROBA-V*, and *MODIS* according to the scope of the research area. The advantage is reducing the workload of data processing (masks are used to confine image processing operations to specific areas in the image. A mask has only two types of pixel values: 0 and non-zero. When the mask raster is applied to a source image, the non-zero pixels are processed, and the 0 pixels are ignored when you perform subsequent image processing operations).

2.3. Methodology

The basic idea of this study was to adopt the *TVDI* to replace the original *SMI* (Soil Moisture Index) to realize downscaling factor optimization and improve SMAP data downscaling. After completing the downscaling process, this study used the control experiment method to compare the downscaling factor method using *TVDI* to the original *SMI* approach based on the same ground control point.

2.3.1. Model Building

Soil moisture downscaling was realized by the downscaling factor; therefore, the downscaling factor was key to the soil moisture scale. The expression for the downscaling factor is shown below [31]:

$$F = \frac{SMI_{high}}{SMI_{low}} \tag{1}$$

where F is the scale factor, SMI_{high} is the soil moisture index at a high resolution, and SMI_{low} is soil moisture at a low resolution.

According to previous studies, the latent heat flux index was used as the *SMI*, which was constructed mainly using temperature, vegetation index, and latent heat flux. The expression of the original *SMI* was as follows [20]:

$$SMI_{high} = 1 - \frac{(1 - \alpha NDVI_{PROBA-V})(T_{MODIS} - T_{min})}{(1 - \alpha NDVI_{PROBA-V})(T_{MODIS\_max} - T_{MODIS\_min}) + (T_e - T_{MODIS\_min})} \tag{2}$$

$$\alpha = 1 - \frac{Q - Q_{min}}{Q_{max} - Q_{min}} \tag{3}$$

where $NDVI_{PROBA-V}$ is the *NDVI* based on *PROBA-V* data, T_{MODIS} is the surface temperature corresponding to *MODIS* data, T_{MODIS_min} is the minimum surface temperature based on *MODIS* in the study area, T_{MODIS_max} is the maximum surface temperature of *MODIS* in the study area, T_e is the maximum surface temperature under complete vegetation cover, Q_{max} is the maximum latent heat flux on the surface, and Q_{min} is the minimum latent heat flux on the surface. *SMI* relates to soil moisture through latent heat flux.

As can be seen from formulas (2) and (3), the surface temperature, vegetation index, and latent heat flux must be obtained to achieve downscaling. As the latent heat flux could not be measured directly, additional inversion experiments were required. Additionally, the *NDVI* description of the area with high vegetation coverage was insufficient [20]. Therefore, this study introduced the *TVDI* to enhance *SMI* performance, which is expressed as:

$$F = \frac{1 - TVDI_{high}}{1 - TVDI_{low}} \tag{4}$$

where $TVDI_{high}$ denotes the *TVDI* in high resolution (0.3 km) using *PROBA-V* and *MODIS* data, and $TVDI_{high}$ is the *TVDI* at low resolution (9 km) using SMAP and *PROBA-V*. The *TVDI* mainly comprises surface temperature and coefficients a, b, and *EVI*, among which *EVI* and surface temperature are relatively easy to obtain. According to the scatter plot (Figure 2) of surface temperature and the vegetation index, the simulation parameters a and b could be estimated using the surface temperature and vegetation coverage with the following expression [32]:

$$TVDI_{high} = \frac{T_{MODIS} - T_{MODIS\_min}}{a_1 + b_1 \times EVI_{PROBA-V} - T_{min}} \tag{5}$$

$$TVDI_{low} = \frac{T_{SMAP} - T_{SMAP\_min}}{a_2 + b_2 \times EVI_{PROBA-V} - T_{min}} \tag{6}$$

In formulas (5) and (6), T_{min} is the minimum surface temperature in the study area, a_1 and b_1 are simulation parameters for dry edges, and a_2 and b_2 are simulation parameters for wet edges. The expression is as follows [33]:

$$Dry\ egde:\ T_{NDVI\_max} = a_1 + b_1 \times Fr \tag{7}$$

$$Wet\ edge:\ T_{NDVI\_min} = a_2 + b_2 \times Fr \tag{8}$$

$$Fr = \left(\frac{NDVI - NDVI_{min}}{NDVI_{max} - NDVI_{min}} \right)^2 \tag{9}$$

where Fr is the vegetation fraction, T_{NDVI_max} is the maximum surface temperature corresponding to the Fr value, and T_{NDVI_min} is the minimum surface temperature corresponding to the Fr value. $NDVI_{max}$ and $NDVI_{min}$ correspond to the maximum and minimum of the *NDVI* values, respectively.

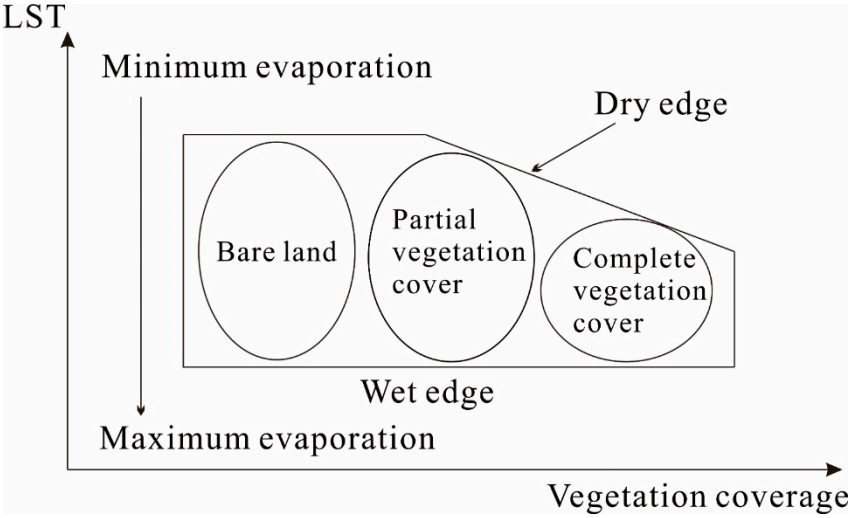

Figure 2. Characteristic space of vegetation coverage and LST (land surface temperature).

Figure 2 shows that under conditions of identical vegetation coverage, soil moisture and surface temperature were inversely related [34]. Based on this principle, a_1, a_2, b_1, and b_2 can be obtained by extracting the vegetation coverage and surface temperature from satellite images and constructing their characteristic space. Parameters a_1 and b_1 were obtained by fitting the dry edge, and parameters a_2 and b_2 were obtained by fitting the wet edge.

TVDI was found to be negatively correlated with soil moisture, and *TVDI* can be substituted into Formula (1); hence, the following expressions are obtained:

$$SM_{high} = SM_{low} \times \frac{1 - TVDI_{high}}{1 - TVDI_{low}} \quad (10)$$

The high-resolution (0.3 km) soil moisture can be obtained by substituting SMAP data in Formula (10).

2.3.2. Validation

The control experiment compared the *TVDI* method with the original *SMI* method. Under the same conditions, four experiments corresponding to four types of land cover were conducted to compare the two methods, and the effects of two methods on SMAP data downscaling were observed.

3. Results

The SMAP data quality will affect the retrieval and the result of downscaling. It is necessary to examine the quality by using the data flags. Bit flags record the ambient surface conditions within each grid cell. These flags provide information as to whether the ground is frozen, open water, dense vegetation, or whether it is permanently covered by snow or ice. The study area mainly includes four types of land cover: wetland, forest, build-up, and cropland; therefore, corresponding surface conditions need to be examined. Whether the surface feature is significant is judged according to the area fraction. For example, the frozen soil flag affects soil moisture retrieval processing in the following ways: (1) if the frozen ground areal fraction is 0.00–0.10, then do not flag, but retrieve soil moisture, (2) if the frozen ground areal fraction is 0.10–0.90, then flag and retrieve soil moisture, (3) if the frozen ground areal fraction is above 0.90, then flag, but do not retrieve soil moisture. In other words, the soil moisture retrieval of no or insignificant feature presence has high quality.

This study examined the data quality of May 2016–May 2017, and found that the proportion of total non-significant pixels was 83.43%, among which the proportion of permanent snow was 92.41%, the proportion of frozen land was 86.61%, the proportion of water surface was 78.76%, the proportion of buildings was 81.21%, and the proportion of dense vegetation was 78.15% (Table 4). It can be found

from the analysis of SMAP quality flags that the data retrieval is of good quality and the use of data is recommended.

Table 4. The proportion of pixels with no or insignificant presence of land cover in study area (%).

	Permanent Snow	Frozen Ground	Surface Water	Built-up Structure	Dense Vegetation
May 2016	93.22	84.60	79.23	81.17	78.24
June 2016	92.16	86.71	76.26	81.55	76.72
July 2016	94.06	91.23	82.65	80.86	75.48
August 2016	91.32	90.38	79.89	81.26	79.33
September 2016	92.27	93.12	77.63	80.26	80.17
October 2016	89.52	88.21	79.46	83.50	77.60
November 2016	91.46	85.81	80.01	83.80	80.33
December 2016	92.29	84.23	78.57	79.59	79.27
January 2017	93.51	83.41	79.06	78.88	78.40
February 2017	93.96	84.81	81.51	82.90	74.64
March 2017	93.79	85.19	76.66	78.79	77.56
April 2017	93.69	83.22	76.03	80.39	77.66
May 2017	90.13	85.01	76.89	82.75	80.60
Avg	92.41	86.61	78.76	81.21	78.15

According to Formula (9), the soil moisture at 0.3 km (SM_{high}) was obtained based on the *TVDI*. The soil moisture map (Figure 3) displays the spatial distribution of the downscaling soil moisture using the *TVDI* as the soil moisture index. In the southwest area of the study site, a region with high soil moisture was observed due to the relatively low *TVDI* of the forest with homogeneous cover, resulting in soil moisture values greater than 0.3.

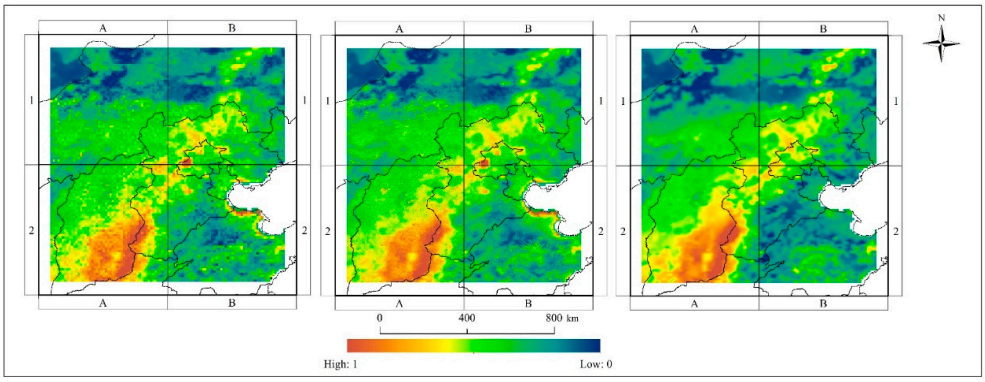

(**a**) (**b**) (**c**)

Figure 3. Downscaling SMAP soil moisture image in the study area at 0.3-km resolution. (**a**) SMAP; (**b**) Proposed method; (**c**) Original method.

The proposed method improved the spatial resolution of the SMAP product from 9 km to 0.3 km. From the experimental results, the image showed a clearer effect after the downscaling process (Figure 3b). Compared with the original method, the proposed method offered a visual effect and greater detail (Figure 3b,c), making it more suitable for a microscale watershed study.

This study selected four sampling areas as the basis for accuracy verification, wherein A1, A2, B1, and B2 correspond respectively to four land types: wetlands, built-up, forest, and cropland. Each sampling area was 9 km × 9 km with 10 ground control points selected as the basis for ground verification. The results of the proposed method and original method are shown in Figures 4 and 5. As can be seen from the display effect, both methods enhanced the spatial resolution of the SMAP product and reflected soil moisture details.

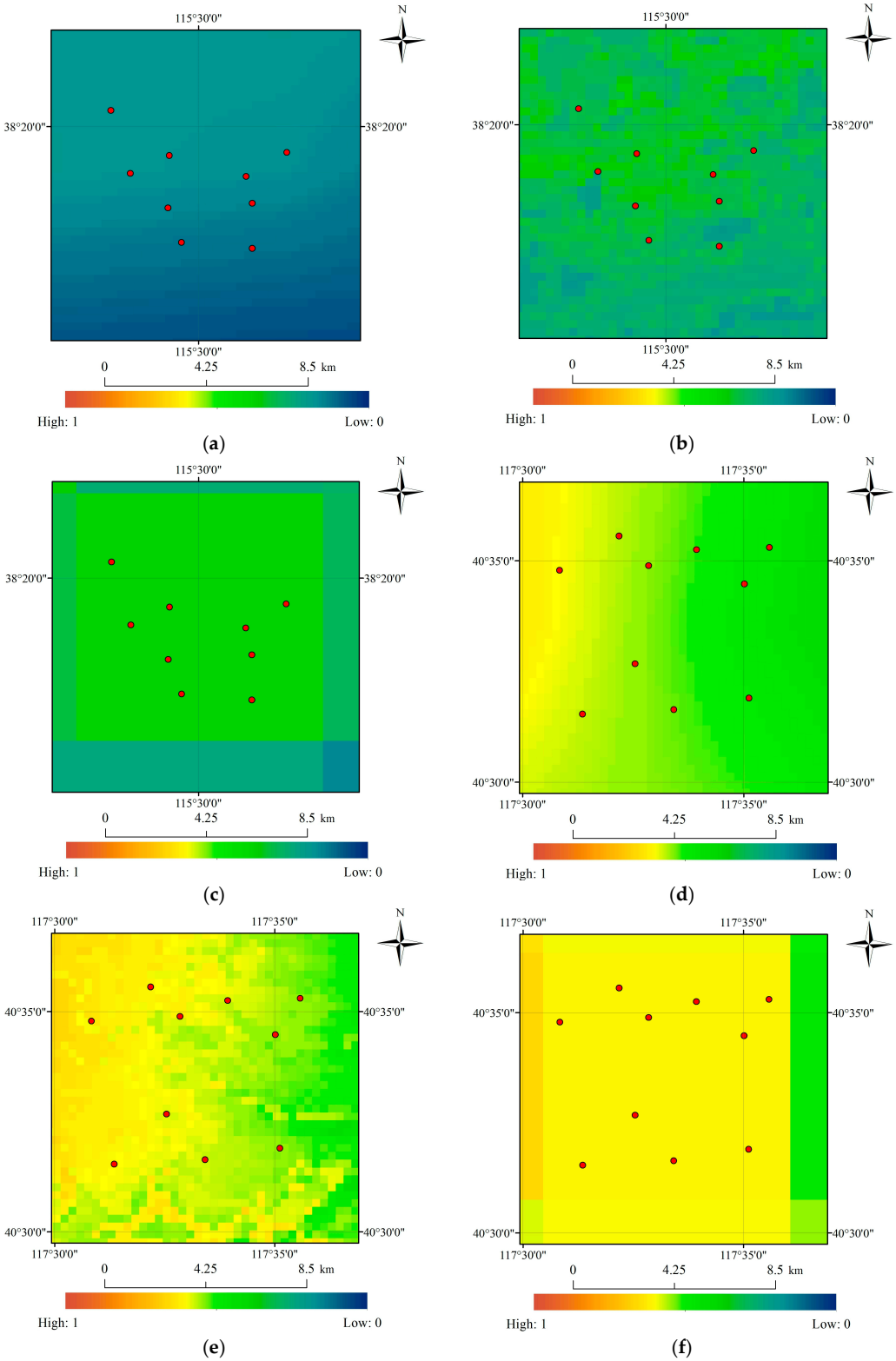

Figure 4. Comparison diagram before and after downscaling process in the sampling area corresponding to A1 and A2, respectively. (**a**) Sample A1 using 9-km resolution SMAP product; (**b**) Sample A1 at 0.3-km resolution after downscaling using the Temperature Vegetation Drought Index (*TVDI*) as downscaling factor; (**c**) Sample A1 at 0.3-km resolution based on the original Soil Moisture Index (*SMI*) method; (**d**) Sample A2 using a 9-km resolution SMAP product; (**e**) Sample A2 at 0.3-km resolution after downscaling using the *TVDI* as the downscaling factor; (**f**) Sample A2 at 0.3-km resolution based on the original *SMI* method.

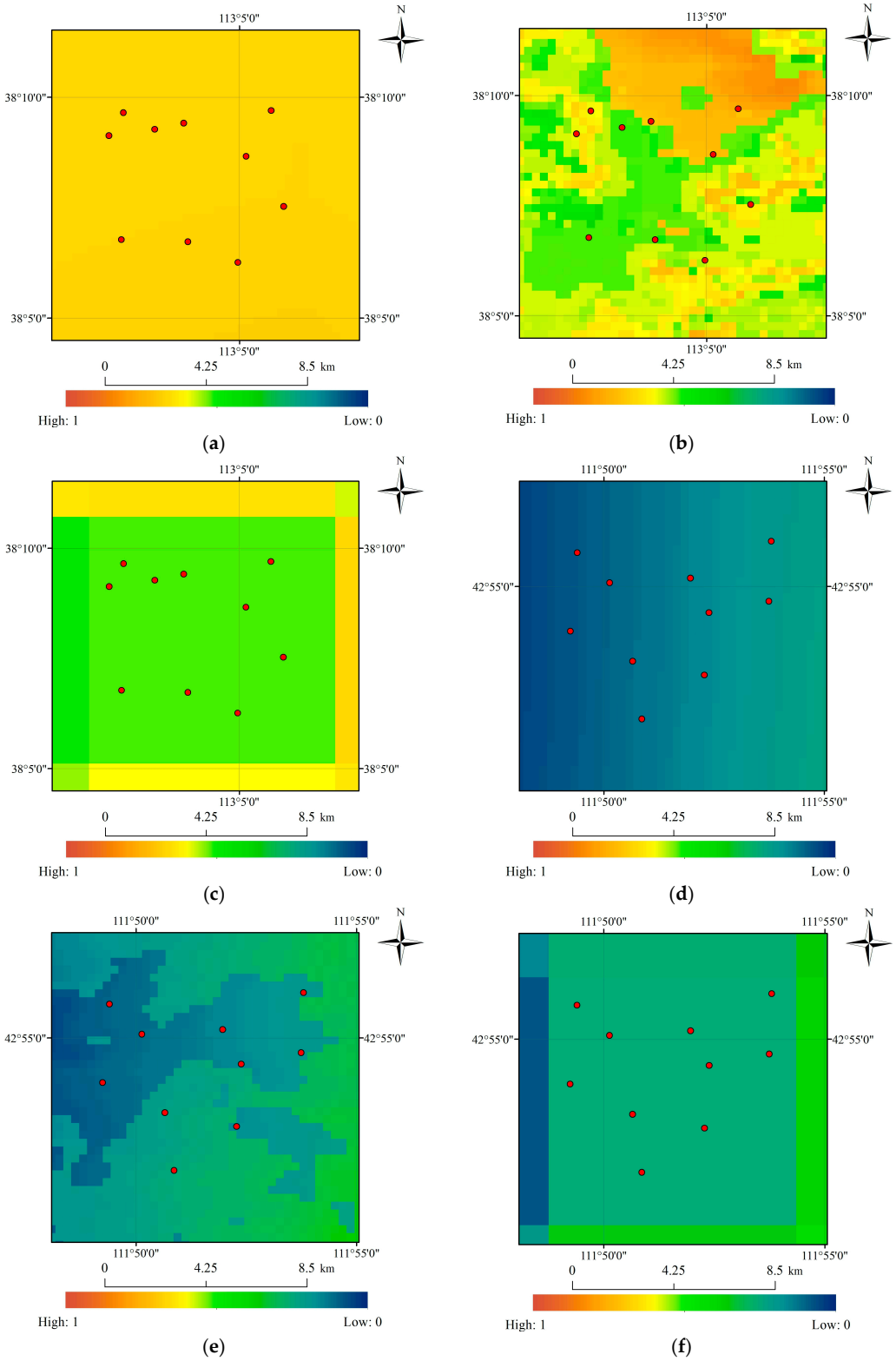

Figure 5. Comparison diagram before and after downscaling process in the sampling area corresponding to B1 and B2, respectively. (**a**) Sample B1 using the 9-km resolution SMAP product; (**b**) Sample B1 at 0.3-km resolution after downscaling using the *TVDI* as the downscaling factor; (**c**) Sample B1 at 0.3-km resolution based on the original *SMI* method; (**d**) Sample B2 using 9-km resolution SMAP product; (**e**) Sample B2 at 0.3-km resolution after downscaling using *TVDI* as the downscaling factor; (**f**) Sample B2 at 0.3-km resolution based on the original *SMI* method.

The second column in Figures 4 and 5 indicate that the improved method can reflect the difference in soil moisture. As can be seen from the comparison of each sampling area, the improved method can better reflect the spatial difference of soil moisture in areas with high vegetation coverage.

Experimental results were analyzed by selecting 10 samples from each sampling area, which revealed that the average error of the sample point scale was higher than that of the SMAP grid scale. Overall, the estimation at a 0.3-km resolution was closer to the observed value, where the root means square error (RMSE) and absolute error (AE) of A1 were greater than that of B1 (Table 5). The error (RMSE and AEF) of area B1 was higher than A2, and the dispersion degree of data was lower than for A2. The error in the A2 region was slightly greater than in B2.

Table 5. Comparison of soil moisture content between the results of downscaling soil moisture at 0.3-km resolution and Level 3 SMAP soil moisture product at 9-km resolution based on field observations of 40 sample plots (unit: $m^3 \cdot m^{-3}$, Stdev: standard deviation, root mean square error (RMSE) (%) = RMSE × 100/sample mean).

Sampling Area (no.)			Downscaling Model Using *TVDI*		Downscaling Model Based on Original *SMI* Method.		Level 3 SMAP Soil Moisture Product in 9 km Resolution	
	Type	Observations ($m^3 \cdot m^{-3}$)	Estimations ($m^3 \cdot m^{-3}$)	Error (%)	Estimations ($m^3 \cdot m^{-3}$)	Error (%)	Estimations ($m^3 \cdot m^{-3}$)	Error (%)
A1(1)	Wetlands	0.1580	0.1669	5.64%	0.1707	8.06%	0.1329	15.89%
A1(2)	Wetlands	0.1771	0.1871	5.66%	0.1912	7.98%	0.1465	17.28%
A1(3)	Wetlands	0.2019	0.2145	6.24%	0.2181	8.03%	0.221	9.46%
A1(4)	Wetlands	0.1932	0.2050	6.12%	0.2090	8.19%	0.164	15.11%
A1(5)	Wetlands	0.1847	0.1972	6.77%	0.1997	8.12%	0.1642	11.10%
A1(6)	Wetlands	0.1467	0.1568	6.91%	0.1570	6.99%	0.1202	18.06%
A1(7)	Wetlands	0.1309	0.1394	6.51%	0.1400	6.96%	0.1055	19.40%
A1(8)	Wetlands	0.1871	0.1994	6.57%	0.2002	7.02%	0.1599	14.54%
A1(9)	Wetlands	0.2027	0.2142	5.67%	0.2180	7.56%	0.2211	9.08%
A1(10)	Wetlands	0.2049	0.2178	6.28%	0.2195	7.12%	0.1711	16.50%
A2(11)	Built-up	0.2992	0.3244	8.41%	0.3274	9.44%	0.2131	28.78%
A2(12)	Built-up	0.2432	0.2616	7.58%	0.2661	9.40%	0.2923	20.19%
A2(13)	Built-up	0.2528	0.2753	8.88%	0.2737	8.26%	0.1922	23.97%
A2(14)	Built-up	0.2268	0.2453	8.15%	0.2478	9.27%	0.2888	27.34%
A2(15)	Built-up	0.2278	0.2455	7.77%	0.2464	8.14%	0.1729	24.10%
A2(16)	Built-up	0.2623	0.2935	11.91%	0.2839	8.25%	0.1893	27.83%
A2(17)	Built-up	0.2871	0.3125	8.84%	0.3134	9.16%	0.2138	25.53%
A2(18)	Built-up	0.2262	0.2439	7.84%	0.2467	9.06%	0.1633	27.81%
A2(19)	Built-up	0.2353	0.2538	7.87%	0.2545	8.14%	0.2798	18.91%
A2(20)	Built-up	0.2272	0.2451	7.89%	0.2491	9.62%	0.1643	27.68%
B1(21)	Forest	0.1124	0.1483	9.31%	0.1493	10.02%	0.1109	1.33%
B1(22)	Forest	0.1343	0.2007	9.48%	0.2028	10.66%	0.1324	1.47%
B1(23)	Forest	0.1198	0.1970	9.25%	0.2010	11.46%	0.1259	5.10%
B1(24)	Forest	0.1160	0.1573	8.39%	0.1617	11.47%	0.1590	37.03%
B1(25)	Forest	0.1159	0.1691	8.59%	0.1733	11.30%	0.1143	1.34%
B1(26)	Forest	0.1101	0.2111	8.85%	0.2141	10.42%	0.1196	8.62%
B1(27)	Forest	0.0991	0.2219	8.58%	0.2249	10.02%	0.1039	4.79%
B1(28)	Forest	0.1287	0.2134	8.86%	0.2185	11.50%	0.1437	11.65%
B1(29)	Forest	0.1186	0.1813	9.32%	0.1834	10.64%	0.1646	38.72%
B1(30)	Forest	0.0992	0.1930	8.18%	0.1982	11.08%	0.1123	13.17%
B2(31)	Cropland	0.1357	0.1414	4.23%	0.1444	6.38%	0.1598	17.73%
B2(32)	Cropland	0.1833	0.1910	4.20%	0.1952	6.47%	0.1549	15.49%
B2(33)	Cropland	0.1803	0.1892	4.91%	0.1939	7.52%	0.1473	18.30%
B2(34)	Cropland	0.1451	0.1512	4.23%	0.1549	6.75%	0.1860	28.21%
B2(35)	Cropland	0.1557	0.1635	5.02%	0.1658	6.46%	0.1337	14.11%
B2(36)	Cropland	0.1939	0.2038	5.08%	0.2062	6.33%	0.1399	27.83%
B2(37)	Cropland	0.2044	0.2147	5.03%	0.2175	6.40%	0.1616	20.96%
B2(38)	Cropland	0.1960	0.2048	4.47%	0.2099	7.07%	0.1681	14.22%
B2(39)	Cropland	0.1658	0.1730	4.35%	0.1761	6.21%	0.1926	16.15%
B2(40)	Cropland	0.1784	0.1860	4.24%	0.1919	7.56%	0.1514	15.14%
Mean =		0.1792	0.1815	6.91%	0.1815	8.83%	0.1680	11.67%
RMSE =			0.0285		0.0298		0.0383	
Stdev =		0.0525	0.0488		0.0485	0.04872	0.0487	

Data source: National Earth Science Data Sharing Infrastructure.

The RMSE was used to measure the deviation between the observed and estimated values. Before the downscaling process, a large deviation was observed between the SMAP product at 9-km resolution and ground observations due to the large scale. The error range of the SMAP soil moisture product and sample point observation value of the four sampling areas was between 0.0260–0.0555 $m^3 \cdot m^{-3}$, and the RMSE was 17.23%–25.38% (Table 6).

Table 6. Comparison of SMAP soil moisture and downscaled result within each sampling area. (AE: absolute error, *NDVI*: Normalized Difference Vegetation Index, RMSE: root mean square error, LST: land surface temperature, RMSE (%) = 100% × AE/Observations).

	Downscaling Model Using *TVDI* as Downscaling Factor		**Downscaling Model Based on Original *SMI* Method.**		**Level 3 SMAP Soil Moisture Product in 9-km Resolution**				
	AE ($m^3 \cdot m^{-3}$)	**RMSE (%)**	**AE ($m^3 \cdot m^{-3}$)**	**RMSE (%)**	**AE ($m^3 \cdot m^{-3}$)**	**RMSE (%)**	**Vegetation Water Content**	**Roughness**	**LST**
A1	0.0112	6.28%	0.0138	7.73%	0.0260	17.77%	0.1320	0.1366	29.9737
A2	0.0218	8.74%	0.0223	8.96%	0.0640	25.38%	0.3281	0.1563	33.0361
B1	0.0156	8.96%	0.0190	10.94%	0.0555	21.00%	0.6930	0.1552	27.0131
B2	0.0081	4.67%	0.0119	6.82%	0.0341	18.10%	0.1844	0.1066	15.3997

After the downscaling process, the estimated value of soil moisture in the sampling area was closer to the observed value. The error range of the downscaled result was between 0.0081–0.0218, with RMSEs of 4.67%–8.74%. In addition, a comparison of the four sampling areas indicated that the improvement of A2 (25.38%–8.74%) in the sampling area was largest, followed by B1 (21.00%–8.96%), B2 (18.10%–4.67%), and A1 (17.77%–6.28%) with the lowest enhancement effect. The vegetation water content derived from the *NDVI* of B1 was greater than 0.6, and its percentage error was 8.96%. The roughness of A2 exceeded 0.155, corresponding to a percentage error of 8.74% (Table 6).

Analysis of the experimental results suggests that the improved method was more accurate than the original. The corresponding vegetation water content values of A2 and B1 were 0.3281 and 0.6930, respectively, and the corresponding errors were higher than A2 and B2, as *NDVI* was used to construct the *TVDI* scaling factor, resulting in an RMSE that was greater than the original method in areas with high vegetation coverage. In addition, the roughness would limit the data quality, A2 and B1 with the high roughness, resulting in an RMSE greater than A1 and B2.

To verify the stability of the downscaling model using the *TVDI*, the proposed method was applied to the long time series of soil moisture (2016–2017). The SMAP data of 12 months were selected after quality flags examination, and the downscaling results were obtained by batch processing. The error percentages of the four sample areas were all 6.74%. Among them, A1 had the smallest range of soil moisture (0.10–0.13), and its mean percentage error was 5.55%. B2 had the largest variation range (0.16–0.26), with a mean percentage error of 5.66%. The range of B1 was between 0.16 and 0.24, with an average error of 7.93%. A2 ranged between 0.20–0.28, with an average error of 7.80% (Figure 6). From the experimental performance of a time series of SMAP, the proposed method had certain stability and can be applied to the scale reduction inversion of a long time series.

Figure 7 shows the spatial characteristics of soil moisture dynamic changes in the study area. The variation is relatively small in the northwestern part of the study area, whose land cover types is mainly in wetlands. In the southeast part of the study area (mainly covered by cropland), the smallest soil moisture occurred in the late winter and spring period (February, March, and April); because winter wheat was in the growing period, the water consumption increased, which made the soil moisture significantly reduced. The largest soil moisture appeared in the precipitation period (July, August, and September). In addition, regarding the change characteristics of the northeastern part and southwestern part, soil moisture in summer was higher than that in winter.

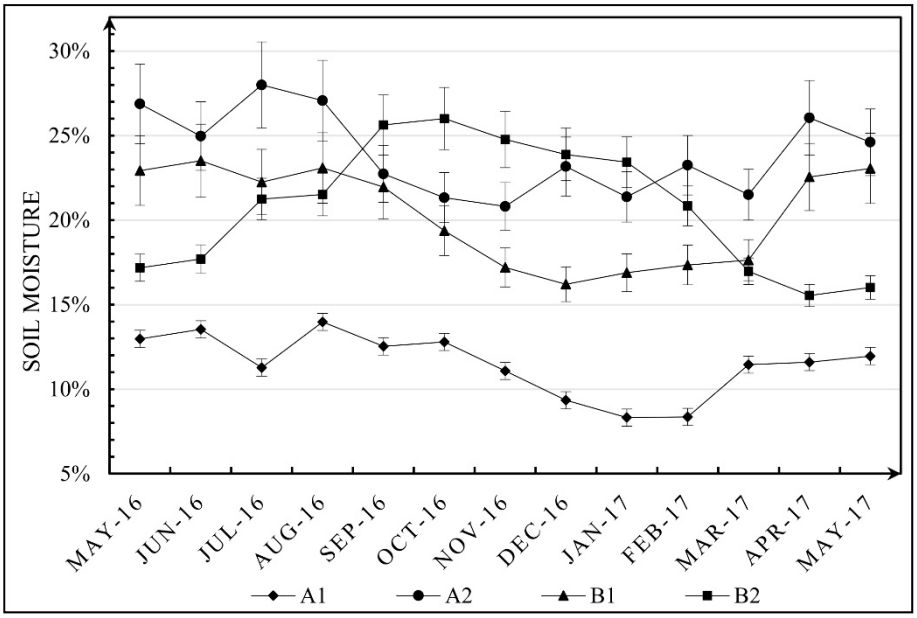

Figure 6. Time series (May 2016–May 2017) of SMAP soil moisture after downscaling using the *TVDI* in four sample areas.

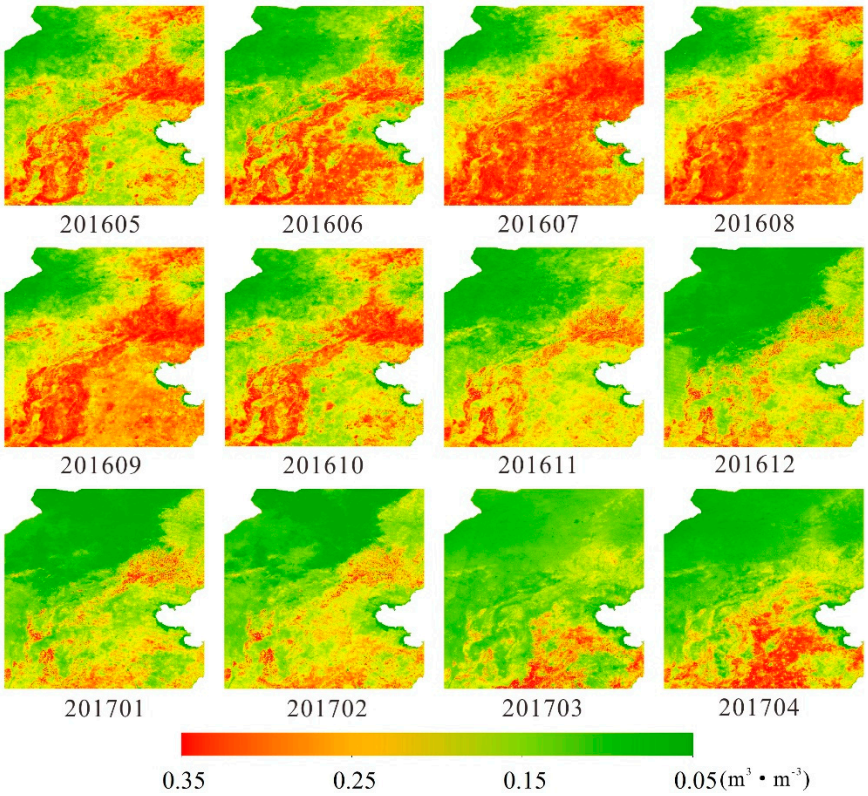

Figure 7. Spatial and temporal distribution of SMAP soil moisture after downscaling in the study area.

4. Discussion

The accuracy of the three models of the downscaling factor model of the *TVDI*, original *SMI*, and regression model were verified through four 9 km × 9 km sampling areas. Table 7 shows that the mean RMSE of the downscaling factor model of the *TVDI* was slightly lower than that of the original *SMI* method, whereas the RMSE of the regression model was higher than the previous two, indicating that the overall effect of the downscaling factor model of the *TVDI* and the original *SMI* method

was close. According to the accuracy of the four sampling areas, the accuracy of the downscaling factor model in A1 and A2 was higher than that of the original *SMI* method. However, for B1 and B2, the accuracy of the original *SMI* method was higher. The types of sampling areas corresponding to A1 and A2 were wetlands and cities, implying that the downscaling factor model of the *TVDI* was more suitable for areas with low vegetation coverage. B1 and B2 corresponded to the sampling areas of forest and cultivated land, making them more suitable for the original *SMI* method. The regression model was simpler and easier to implement, but it was less accurate than the other two methods. The R^2 of the regression model downscaling results was lower than that of the downscaling method, indicating that the estimated value after downscaling was closer to the observed value, but the degree of model fit was reduced.

Table 7. Comparison of accuracy verification effect of soil moisture downscaling model.

Sample Area	Downscaling Soil Moisture Using *TVDI*	Original *SMI* Method	Regression Model		Level 3 SMAP SOIL MOISTURE at 9-km Resolution
	RMSE	RMSE	RMSE	R^2	
A1	0.0112	0.0138	0.0150	0.4752	0.0260
A2	0.0218	0.0223	0.0257	0.5387	0.0640
B1	0.0156	0.0190	0.0209	0.5095	0.0555
B2	0.0081	0.0119	0.0146	0.5291	0.0341
Mean =	0.0142	0.0167	0.0190	0.5131	0.0449

The experimental error of wetland and grassland was greater than that of other land-cover types. The second reason for the error distribution involved the complexity of land-cover types. The A2 area contained urban, cropland, and mixed forests, and the land-cover type was more than B2 (mainly cultivated land); accordingly, the error of A2 was greater than that of B2. Additionally, the existence of mixed pixels was a cause of error, as evidenced by the error in the SMAP grid scale being greater overall than that in the sampling scale. Thus, the land-cover type appeared to be one of the impressive factors in the downscaling treatment, and the influence of wetland and cultivated land was more obvious (Figure 8). The downscaled results generally improved the description of spatial differentiation patterns, and can be applied to hydrological studies at the watershed scale.

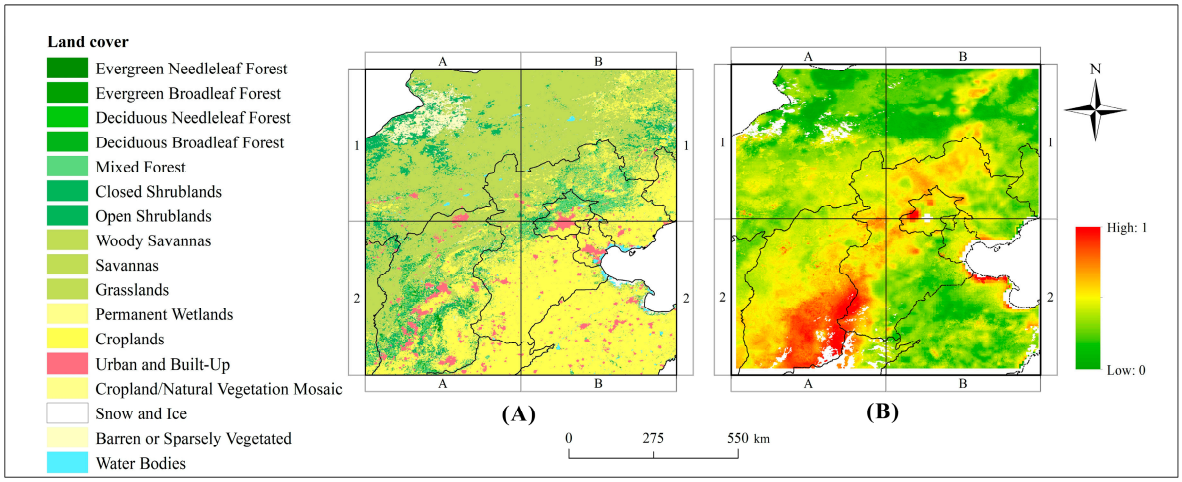

Figure 8. Land-cover reference and downscaling results of soil moisture. (**A**) Land cover types in the study area; (**B**) Soil moisture at 0.3-km resolution after downscaling using the *TVDI* as the downscaling factor.

5. Conclusions

The low resolution of the existing remote sensing soil moisture products render them unable to meet the needs of regional or watershed research. Therefore, soil moisture downscaling is potentially highly valuable for image applications. In this paper, a 9-km spatial resolution of the SMAP soil moisture product was conducted by a downscaling factor, and soil moisture data at 0.3-km spatial resolution were obtained. Accuracy was verified based on sampling points; the results suggested that *TVDI* can be used as a downscaling factor to reflect the spatial differentiation of soil moisture in SMAP product pixels, possessing great clinical significance in subsequent watershed hydrology studies (especially for improving the spatial resolution of SMAP products). Likely main sources of error included SMAP soil moisture products and land-cover types; the error of downscaling treatment in wetland and cropland was greater than that of forest. In the process of building the model, it is best to avoid these errors as much as possible. No evidence indicates that the wet and dry edge fitting of the *TVDI* influenced the downscaling results, which warrant further study.

Author Contributions: Conceptualization, A.-X.Z.; Data curation, S.-D.F. and Z.-H.L.; Formal analysis, B.L.; Funding acquisition, Y.-M.H.; Investigation, Z.S., W.-B.W. and Y.-C.P.; Methodology, S.-D.F., Z.-H.L., G.-X.W. and A.-X.Z.; Project administration, Y.-M.H.; Resources, L.W.; Software, W.-B.W. and B.L.; Supervision, Y.-M.H., L.W., G.-X.W., A.-X.Z. and B.L.; Validation, Z.S. and Y.-C.P.; Writing original draft, S.-D.F.; Writing review & editing, S.-D.F. and G.-X.W.

Funding: This research was funded by Guangdong Provincial Science and Technology Plan Project (2017B090907030), Qinghai Province Science and Technology Plan Project (2017-ZJ-730), Guangzhou Science and Technology Plan Project (201804020034, 201807010048), and the Science and Technology Planning Project of Guangdong Province (2014A050503060).

Acknowledgments: This work was supported by a grant from College of Natural Resources and Environment (South China Agricultural University). The authors would like to thank Z.-H.L. for excellent technical support and A.-X.Z. for critically reviewing the manuscript.

Conflicts of Interest: The authors declare no conflict of interest.

References

1. Kuenzer, C.; Gessner, U.; Wagner, W. *Soil Moisture from Thermal Infrared Satellite Data: Synergies with Microwave Data*; Springer: Amsterdam, The Netherlands, 2013; pp. 315–330.
2. Seneviratne, S.I.; Davin, E.; Hirschi, M.; Mueller, B.; Orlowsky, B.; Teuling, A. Soil Moisture-Ecosystem-Climate Interactions in a Changing Climate. In Proceedings of the AGU Fall Meeting, San Francisco, CA, USA, 5–9 December 2011.
3. Vrugt, J.A.; Gupta, H.V.; Dekker, S.C.; Sorooshian, S.; Wagener, T.; Bouten, W. Application of stochastic parameter optimization to the Sacramento Soil Moiture Accounting Model. *J. Hydrol.* **2006**, *325*, 288–307. [CrossRef]
4. Frey, M.P.; Stamm, C.; Schneider, M.K.; Reichert, P. Using discharge data to reduce structural deficits in a hydrological model with a Bayesian inference approach and the implications for the prediction of critical source areas. *Water Resour. Res.* **2011**, *47*, 12529. [CrossRef]
5. Me, W.; Abell, J.M.; Hamilton, D.P. Effects of hydrologic conditions on SWAT model performance and parameter sensitivity for a small, mixed land use catchment in New Zealand. *Hydrol. Earth Syst. Sci.* **2015**, *19*, 4127–4147. [CrossRef]
6. Entekhabi, D.; Njoku, E.; O'Neill, P. The Soil Moisture Active and Passive Mission (SMAP): Science and applications. In Proceedings of the IEEE Radar Conference, Pasadena, CA, USA, 4–8 May 2009.
7. Spencer, M.; Wheeler, K.; Chan, S.; Piepmeier, J.; Hudson, D.; Medeiros, J. The planned Soil Moisture Active Passive (SMAP) mission L-band radar/radiometer instrument. In Proceedings of the Geoscience and Remote Sensing Symposium, Vancouver, BC, Canada, 24–29 July 2011.
8. Chauhan, N.S.; Miller, S.; Ardanuy, P. Spaceborne soil moisture estimation at high resolution: A microwave-optical/IR synergistic approach. *Int. J. Remote Sens.* **2003**, *24*, 4599–4622. [CrossRef]

9. Ray, R.L.; Jacobs, J.M.; Cosh, M.H. Landslide susceptibility mapping using downscaled AMSR-E soil moisture: A case study from Cleveland Corral, California, US. *Remote Sens. Environ.* **2010**, *114*, 2624–2636. [CrossRef]
10. Merlin, O.; Bitar, A.A.; Walker, J.P.; Kerr, Y. An improved algorithm for disaggregating microwave-derived soil moisture based on red, near-infrared and thermal-infrared data. *Remote Sens. Environ.* **2010**, *114*, 2305–2316. [CrossRef]
11. Kim, J.; Hogue, T.S. Improving Spatial Soil Moisture Representation Through Integration of AMSR-E and MODIS Products. *IEEE Trans. Geosci. Remote Sens.* **2012**, *50*, 446–460. [CrossRef]
12. Aman, A.; Randriamanantena, H.P.; Podaire, A.; Frouin, R. Upscale integration of normalized difference vegetation index: The problem of spatial heterogeneity. *IEEE Trans. Geosci. Remote Sens.* **1992**, *30*, 326–338. [CrossRef]
13. Mayaux, P.; Lambin, E.F. Estimation of tropical forest area from coarse spatial resolution data: A two-step correction function for proportional errors due to spatial aggregation. *Remote Sens. Environ.* **1995**, *53*, 1–15. [CrossRef]
14. Munechika, C.K.; Warnick, J.S.; Salvaggio, C.; Schott, J.R. Resolution Enhancement of Multispectral Image Data to Improve Classification Accuracy. *Photogramm. Eng. Remote Sens.* **1993**, *59*, 67–72.
15. Sun, H.; Zhao, X.; Chen, Y.; Gong, A.; Yang, J. A new agricultural drought monitoring index combining MODIS NDWI and day–night land surface temperatures: A case study in China. *Int. J. Remote Sens.* **2013**, *34*, 8986–9001. [CrossRef]
16. Merlin, O.; Walker, J.P.; Chehbouni, A.; Kerr, Y. Towards deterministic downscaling of SMOS soil moisture using MODIS derived soil evaporative efficiency. *Remote Sens. Environ.* **2008**, *112*, 3935–3946. [CrossRef]
17. Rahimzadeh-Bajgiran, P.; Berg, A.A.; Champagne, C.; Omasa, K. Estimation of soil moisture using optical/thermal infrared remote sensing in the Canadian Prairies. *Isprs J. Photogramm. Remote Sens.* **2013**, *83*, 94–103. [CrossRef]
18. Ye, N.; Walker, J.P.; Guerschman, J.; Ryu, D.; Gurney, R.J. Standing water effect on soil moisture retrieval from L-band passive microwave observations. *Remote Sens. Environ.* **2015**, *169*, 232–242. [CrossRef]
19. Loew, A.; Schlenz, F. A dynamic approach for evaluating coarse scale satellite soil moisture products. *Hydrol. Earth Syst. Sci. Discuss.* **2010**, *7*, 75–90. [CrossRef]
20. Jiang, L.; Islam, S. An intercomparison of regional latent heat flux estimation using remote sensing data. *Int. J. Remote Sens.* **2003**, *24*, 2221–2236. [CrossRef]
21. Yang, Y.; Yang, Y.; Moiwo, J.P.; Hu, Y. Estimation of irrigation requirement for sustainable water resources reallocation in North China. *Agric. Water Manag.* **2010**, *97*, 1711–1721. [CrossRef]
22. Liu, P.W.; Judge, J.; Roo, R.D.D.; England, A.W.; Bongiovanni, T. Uncertainty in Soil Moisture Retrievals Using the SMAP Combined Active–Passive Algorithm for Growing Sweet Corn. *IEEE J. Sel. Top. Appl. Earth Obs. Remote Sens.* **2016**, *9*, 3326–3339. [CrossRef]
23. Derksen, C.; Xu, X.; Dunbar, R.S.; Colliander, A.; Kim, Y.; Kimball, J.S.; Black, T.A.; Euskirchen, E.; Langlois, A.; Loranty, M.M. Retrieving landscape freeze/thaw state from Soil Moisture Active Passive (SMAP) radar and radiometer measurements. *Remote Sens. Environ.* **2017**, *194*, 48–62. [CrossRef]
24. Francois, M.; Santandrea, S.; Mellab, K.; Vrancken, D.; Versluys, J. The PROBA-V mission: The space segment. *Int. J. Remote Sens.* **2014**, *35*, 2548–2564. [CrossRef]
25. Dierckx, W.; Sterckx, S.; Benhadj, I.; Livens, S.; Duhoux, G.; Achteren, T.V.; Francois, M.; Mellab, K.; Saint, G. PROBA-V mission for global vegetation monitoring: Standard products and image quality. *Int. J. Remote Sens.* **2014**, *35*, 2589–2614. [CrossRef]
26. Hansen, M.C.; Reed, B.; Defries, R.S.; Belward, A.S. A comparison of the IGBP DISCover and University of Maryland 1 km global land cover products. *Int. J. Remote Sens.* **2000**, *21*, 1365–1373. [CrossRef]
27. Loveland, T.R.; Reed, B.C.; Brown, J.F.; Ohlen, D.O.; Zhu, Z.; Yang, L.; Merchant, J.W.; Defries, R.S.; Belward, A.S. Development of a global land cover characteristics database and IGBP DISCover from 1 km AVHRR data. *Int. J. Remote Sens.* **2000**, *21*, 1303–1330. [CrossRef]
28. Johansen, K.; Tiede, D.; Blaschke, T.; Arroyo, L.A.; Phinn, S. Automatic Geographic Object Based Mapping of Streambed and Riparian Zone Extent from LiDAR Data in a Temperate Rural Urban Environment, Australia. *Remote Sens.* **2011**, *3*, 1139–1156. [CrossRef]

29. Aryal, J.; Josselin, D.; Papajorgji, P. Environmental Object Recognition in a Natural Image: An Experimental Approach Using Geographic Object-Based Image Analysis (GEOBIA). *Int. J. Agric. Environ. Inf. Syst.* **2014**, *5*, 1–18. [CrossRef]
30. Fan, S.; Liu, Z.; Hu, Y. Extraction of building information using geographic object-based image analysis. In Proceedings of the International Workshop on Earth Observation and Remote Sensing Applications, Guangzhou, China, 4–6 July 2016.
31. Choi, M.; Hur, Y. A microwave-optical/infrared disaggregation for improving spatial representation of soil moisture using AMSR-E and MODIS products. *Remote Sens. Environ.* **2012**, *124*, 259–269. [CrossRef]
32. Sandholt, I.; Rasmussen, K.; Andersen, J. A simple interpretation of the surface temperature/vegetation index space for assessment of surface moisture status. *Remote Sens. Environ.* **2002**, *79*, 213–224. [CrossRef]
33. Goward, S.N.; Xue, Y.; Czajkowski, K.P. Evaluating land surface moisture conditions from the remotely sensed temperature/vegetation index measurements : An exploration with the simplified simple biosphere model. *Remote Sens. Environ.* **2002**, *79*, 225–242. [CrossRef]
34. Wang, P. Using MODIS Land Surface Temperature and Normalized Difference Vegetation Index products for monitoring drought in the southern Great Plains, USA. *Int. J. Remote Sens.* **2004**, *25*, 61–72.